Pressure control of the spin reorientation transition in the rare-earth orthoferrite $YbFeO_3$

S. A. Skorobogatov,[1,2] L. S. Wu,[3,4] T. Xie,[5] K. A. Shaykhutdinov,[1,2] E. V. Pomjakushina,[6] A. Podlesnyak,[5] and S. E. Nikitin[7,*]

[1]*Kirensky Institute of Physics, Federal Research Center KSC SB RAS, Krasnoyarsk 660036, Russia*
[2]*Department of Solid State Physics and Nanotechnology, Institute of Engineering Physics and Radioelectronics, Siberian Federal University, Krasnoyarsk 660041, Russia*
[3]*Department of Physics, Southern University of Science and Technology, Shenzhen 518055, China*
[4]*Shenzhen Key Laboratory of Advanced Quantum Functional Materials and Devices, Southern University of Science and Technology, Shenzhen 518055, China*
[5]*Neutron Scattering Division, Oak Ridge National Laboratory, Oak Ridge, Tennessee 37831, USA*
[6]*Laboratory for Multiscale Materials Experiments, Paul Scherrer Institut, CH-5232 Villigen PSI, Switzerland*
[7]*Laboratory for Neutron Scattering and Imaging, Paul Scherrer Institut, CH-5232 Villigen-PSI, Switzerland*

(Received 31 May 2023; accepted 7 August 2023; published 23 August 2023)

$YbFeO_3$ is exceptional among the rare-earth orthoferrites for having the lowest spin-reorientation transition (SRT) temperature, $T_{SRT} \simeq 8$ K, which makes it particularly appealing to examine the interplay between non-collinear magnetism of the Fe sublattice and quasi-one-dimensional XXZ effective $S = 1/2$ chains of Yb^{3+} moments. Our paper focuses on the magnetic dynamics of $YbFeO_3$ using inelastic neutron scattering (INS), at temperatures below and above the SRT, under an applied hydrostatic pressure of 2 GPa, and in magnetic fields up to 4 T. The low-energy zero-field excitation spectrum at ambient pressure and temperatures below the SRT is dominated by a gapped magnon mode of the Yb subsystem at 0.84 meV with a dispersion only in the [00L] direction. Above T_{SRT}, a continuum appears on top of the magnon mode because of temperature population of the magnon band, and the gap decreases to around 0.4 meV. The INS spectra in the magnetic field, both above and below T_{SRT}, are characterized by two well-separated gapped modes. The SRT is clearly visible at low fields $B < 1$ T, but it gradually disappears at higher magnetic fields. The hydrostatic pressure of $p = 2$ GPa effectively reduces the transition width, ΔT_{SRT}, and keeps the SRT at higher fields up to $B \simeq 3$ T. We discuss the effect of the applied pressure in the frame of the modified mean-field theory and show that in the vicinity of the T_{SRT} the pressure tunes the fourth-order anisotropy constant that effectively reduces the ΔT_{SRT}.

DOI: 10.1103/PhysRevB.108.054432

I. INTRODUCTION

The family of rare-earth orthorhombic perovskites has been the subject of active research due to their various fascinating physical phenomena and technological applications [1]. Among these materials, the rare-earth orthoferrites, $RFeO_3$ (R is a rare-earth ion) have attracted particular attention owing to large linear magnetoelectric effect, extraordinary ferroelectricity, anisotropic magnetic entropy change, and strong magnetostriction [2–6]. Besides, the spin-reorientation transition (SRT) of the iron sublattice, governed by the competition between the Zeeman energy, the magnetocrystalline anisotropy, and the Dzyaloshinskii-Moriya (DM) interaction, is an essential physical phenomenon for ultrafast spin switch technology [7,8]. As the temperature decreases, in most orthoferrites with a magnetic R ion, a spontaneous SRT takes place from the $\Gamma 4$ magnetic phase, with Fe moments aligned along the a axis to the $\Gamma 2$ phase and with Fe moments along the c axis (see inset in Fig. 1) [9–11]. The transition temperature T_{SRT} varies dramatically for compounds with different R ions, indicating a key role of the weak R-Fe exchange interaction, J_{R-Fe}, in the magnetic ground state of the iron sublattice.

$YbFeO_3$ crystallizes in an orthorhombic distorted perovskite structure [*Pbnm* (62) space group] with only one type of Fe^{3+} ion octahedrally coordinated with O^{2-} ions [12]. The iron magnetic sublattice orders in a canted antiferromagnetic structure at high temperature $T_N \simeq 630$ K [5]. The magnetic structure is almost collinear and has a small spin canting caused by the DM interaction that induces a weak net ferromagnetic (FM) moment. The Yb sublattice is polarized by this net FM moment of the Fe subsystem but does not magnetically order down to the lowest temperatures, in contrast to isostructural $YbAlO_3$ that exhibit magnetic order below $T_N = 0.88$ K [13]. The eightfold $J = 7/2$ ($L = 3$, $S = 1/2$) multiplet of Yb^{3+} is split into four doublets because of the crystal electric field (CEF) effect. The ground state is well separated from the first excited state $\Delta_{CEF} \approx 20$ meV [14]. Therefore, the low-temperature properties ($k_B T \ll \Delta_{CEF}$) could be described with a pseudospin $S = 1/2$, whereas a real value of the magnetic moment is absorbed into the effective anisotropic g factor.

*Corresponding author: stanislav.nikitin@psi.ch

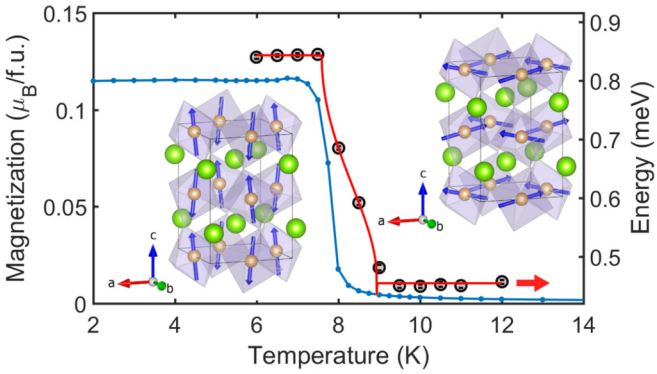

FIG. 1. Temperature dependence of the magnetization of $YbFeO_3$ measured at $B = 0.005$ T along the a axis (blue line). The hollow black circles are the experimental data of the gap in the excitation spectrum at $\mathbf{Q} = (001)$ reciprocal lattice units in zero field and ambient pressure. The solid red line is fit to the modified mean-field theory (see text). Insets: Schematic magnetic structures of the iron sublattice below (left) and above (right) the SRT. Yellow and green spheres represent Fe and Yb ions, respectively. The octahedra denote the oxygen coordination environment.

Recent inelastic neutron scattering (INS) study on $YbFeO_3$ at ambient pressure reveals that the Yb moments are coupled in quasi-one-dimensional XXZ spin chains [14,15]. While the high-energy spin-wave modes of the Fe magnetic sublattice with an energy scale of $E \approx 60$ meV are almost unaffected by the SRT, the low-dimensional spin dynamics of the highly anisotropic Yb subsystem significantly changes on cooling through the SRT. Below T_{SRT}, Yb moments are fully polarized by the effective Fe field, giving rise to the conventional magnon [see Fig. 2(a)]. Above T_{SRT}, an effective field is transverse to the easy axis, leading to the nonpolarized ground state and the rise of a broad continuum above the single-particle mode in the excitation spectrum [see Fig. 2(b)].

High pressure and magnetic field are powerful nonthermal tools to tune the spin-spin correlations. An external magnetic field interferes with the Fe effective field and the hydrostatic pressure is an efficient way to enhance/decrease the couplings of the Yb and Fe moments by changing the bond lengths and bond angles. Here, the effect of the magnetic field on the low-energy magnetic excitation of $YbFeO_3$ as probed by INS at $p = 0$ and 2 GPa is presented. Using the modified mean-field theory [11,16–21] we construct an effective model describing the main features of the evolution of the Yb magnetic spectra in the vicinity of SRT.

II. EXPERIMENTAL DETAILS

A high-quality crystal of $YbFeO_3$ with a mosaicity $\approx 1^\circ$ was grown by the floating-zone method. Before this experiment, the sample prepared from the same crystal was successfully used in the INS experiment at ambient pressure as described in [14]. Magnetization measurements were done using a vibrating-sample magnetometer MPMS-3. For the high-pressure INS experiment, ≈0.1 g single crystal was mounted in a (HHL) horizontal scattering plane and placed in a Teflon tube inside a clamp piston-cylinder NiCrAl pressure cell [22]. The pressure cell was sealed at room temperature and Fluorinert FC-770 was employed as a pressure-transmitting medium to establish a hydrostatic regime. The cell provides optical access to the sample space, allowing instantaneous pressure determination during sample loading using ruby fluorescence monitoring. Note, we did

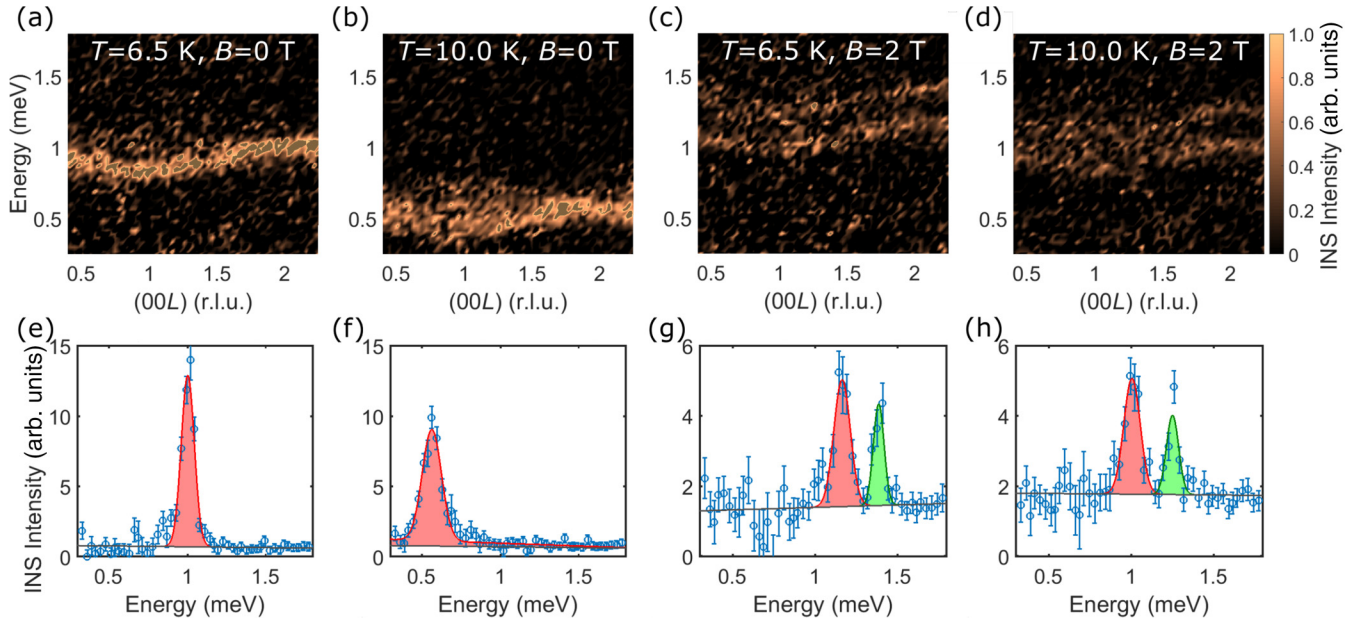

FIG. 2. Effect of temperature and magnetic field on the low-energy excitation spectra of $YbFeO_3$. Color contour plots of the experimental spectrum along the $(00L)$ direction (top) and corresponding energy cuts (bottom) at $\mathbf{Q} = (002)$ measured in pressure $p = 2$ GPa at $T = 6$ K (a), (c), (e), (g), 10 K (b), (d), (f), (h), and magnetic field $B = 0$ T (a), (b), (e), (f) and 2 T (c), (d), (g), (h). The x axis in panels (a)–(d) is shown in reciprocal lattice units. The intensity corresponds to the neutron count rate in arbitrary units after subtraction of nonmagnetic background and normalization.

not monitor pressure during measurements. The pressure of 2.0 GPa was estimated taking into account 10% pressure loss while cooling down to $T = 6$ K.

The INS experiment was carried out using the time-of-flight Cold Neutron Chopper Spectrometer [23,24] at the Spallation Neutron Source at the Oak Ridge National Laboratory. The measurements were done using the rotating single-crystal method at different temperatures (T), magnetic fields (B), and pressures $p = 0$ (ambient) and 2 GPa in a vertical cryomagnet. The INS data were corrected for detector efficiency and transformed from time-of-flight and instrument coordinates to a four-dimensional scattering-intensity function $I(\mathbf{Q}, E)$, where $\mathbf{Q}$ is the momentum transfer and E is the energy transfer. For data reduction and analysis we used the MANTID [25], HORACE [26], and DAVE [27] software packages.

III. RESULTS AND ANALYSIS

According to previous thermodynamic and INS measurements taken at ambient pressure, the Yb moments in $YbFeO_3$ and isostructural $YbAlO_3$ form spin chains running along the c axis despite the three-dimensional perovskite structure [13,14,28]. The INS excitations have weak dispersion in the ab plane compared to the c direction. Therefore, for the current paper we choose the (HHL) as a horizontal scattering plane, i.e., the vertical magnetic field is along the $[1\bar{1}0]$ direction. Note that the Yb moments have a strong Ising-like anisotropy and lie in the ab plane forming an angle within $\alpha \approx \pm 21^\circ$ to the a axis.

Representative experimental spectra at pressure $p =$ 2 GPa, for temperatures below and above SRT, are shown in Figs. 2(a)–2(d). Measuring in a pressure cell considerably reduces the intensity due to small volume of the sample and high background scattering. The statistics is insufficient to make a definitive statement about the weak dispersionless excitation and a continuum above the sharp primary mode, which were observed in ambient pressure at temperatures below SRT [14]. Therefore, the current paper focuses on the dominant low-energy high-intensity branch.

Both spectra, at ambient pressure and at $p = 2$ GPa, look similar. Zero-field spectra below SRT are characterized by a single sharp mode with the gap $\Delta E = 0.844(6)$ meV. The maximum dispersion at the Γ point, $\mathbf{Q} = (002)$, is reached at 1.01(1) meV. Increasing temperature above SRT lowers the gap of this magnonlike mode to $\Delta E \approx 0.4$ meV. Additionally, the scattering continuum arises on the top of the sharp excitation [see Figs. 2(b)]. As shown in Figs. 2(c) and 2(d), the magnetic field $\mathbf{B}||[110]$ splits the one-particle magnon mode into two parallel branches. This happens due to an anisotropy of the Yb moments, which sets up the easy axis in the ab plane with $\alpha \approx \pm 21^\circ$ to the a axis [14]. In this case, the Yb magnetic moments with canting $+21^\circ$ are aligned almost along the direction of the applied field $\mathbf{B}||[110]$, while the second sublattice with easy axis -21° is nearly perpendicular (see inset in Fig. 3). The energy of Yb excitation splits with the applied magnetic field because of the different projections of the easy axis of magnetic moments on the field direction.

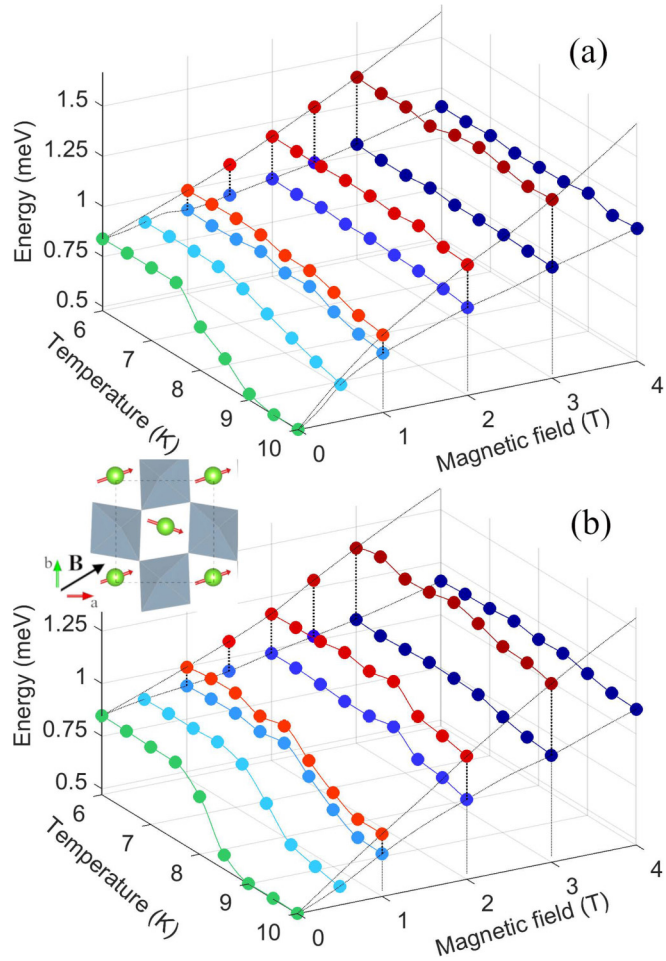

FIG. 3. Temperature and magnetic field dependence of the energy of magnon excitation at $\mathbf{Q} = (001)$, measured at (a) ambient pressure and (b) $p = 2$ GPa. The solid and dotted lines are guides to the eyes to track the temperature evolution of SRT and field splitting of the magnon modes, respectively. Inset: Sketch of the field-induced magnetic structure of the Yb sublattice below T_{SRT} and the direction of the external magnetic field.

One can see that the excitation at $\mathbf{Q} = (002)$ is free from the spin continuum contribution at all relevant temperatures and consists of the sharp magnon mode only. Therefore, to analyze the multiparametric field-pressure-temperature dependence of the magnon branch we take energy cuts at constant $\mathbf{Q} = (002)$ and fit them to a Gaussian function [see Figs. 2(e)–2(h)]. Note that the parameters of the magnon dispersion can be recalculated for any $\mathbf{q}$ using the empirical expression for the tight-binding-like dispersion of a linear chain, $\hbar\omega(q_L) = \Delta_1 + W\cos(\frac{\pi}{2}q_L)^2$, where Δ_1 is the spin gap at $\mathbf{Q} = (001)$ and W is the magnon bandwidth.

The obtained data were used to derive the values of the energy gap of magnon excitation, Δ_1, at $\mathbf{Q} = (001)$ as a function of the magnetic field and temperature, as summarized in Fig. 3. The data at ambient pressure [see Fig. 3(a)] at zero field (green line) show a continuous decrease of the energy gap across the T_{SRT}. As the energy gap evolution with temperature and magnetic field reflects the SRT behavior, we use the Δ_1

in order to estimate both the transition temperature T_{SRT} and transition width ΔT_{SRT}.

An external magnetic field has a dual effect on the spectrum. First, the magnetic field splits the magnon mode into two components whose energies continuously increase with the field. The splitting of the modes is enlarging, since the upper branch rises up at a higher rate compared to the lower one. As we already noted, this happens because the Zeeman splitting is greater for the magnetic moment which has a larger projection on the field direction. Second, the application of the magnetic field rapidly declines the dip of the energy gap above the SRT. Already in the magnetic field $B = 1$ T the transition is hardly visible [blue line in Fig. 3(a)] and it completely washes out at higher magnetic fields.

A qualitatively similar behavior is observed for the data collected under pressure $p = 2$ GPa [see Fig. 3(b)]. Evolution of the energy gap as a function of magnetic field and temperature does not reveal essential differences compared to the ambient pressure data. Nevertheless, there are two apparent changes in the spectra.

(i) The transition width ΔT_{SRT} decreases under pressure. This goes against common expectations. Due to nonhydrostatic effects pressure application actually should make a transition broader. This behavior is also in contrast to the influence of the magnetic field, which increases the transition width with the applied field. We discuss this point in more detail in Sec. IV.

(ii) The critical field B_{crit}, where the energy gap becomes nearly independent of temperature, is higher for the pressurized sample. In Fig. 3(b) we see the evident dip of the energy gap at $T \sim T_{\mathrm{SRT}}$ even at $B = 2$ T. At ambient pressure, as we mentioned above, the transition disappears at $B \approx 1$ T already. This happens because at temperatures above T_{SRT} an effective field of the Fe net moment reorients transverse to the Yb magnetic moments, which should lead to the nonpolarized ground state and continuous spectrum consequently. Despite this, the Yb sublattice is polarized and the weak FM net moment of the Fe subsystem is rotated by the external magnetic field that is parallel to the [110] direction. This ensures that the gap value remains constant for temperatures higher than T_{SRT}.

We finally note that T_{SRT} deduced for both datasets ($p = 0, 2$ GPa) measured with the pressure cell is about 0.5 K larger than that determined in the experiments without the pressure cell as can be seen in Fig. 1. We associate this discrepancy with the thermal gradient between the sample inside the massive pressure cell and the thermal sensor that was fixed on the sample stick. However, because we performed measurements in the pressure cell at $p = 0$ and 2 GPa under identical conditions, this issue appears systematically in both datasets and we can perform accurate comparative analysis to isolate the effect of pressure on the magnetic phase diagram.

IV. DISCUSSION

We discuss the pressure-induced evolution of the ΔT_{SRT} in the $YbFeO_3$ observed in our INS spectra. The interaction of the Fe and Yb magnetic subsystems can be described in terms of an effective field and the modified mean-field theory [11,16–21]. The key idea is that the weak net FM moment of the Fe subsystem polarizes the paramagnetic Yb subsystem, which, in turn, has a significant anisotropy of magnetic susceptibility. Following the modified mean-field theory the system close to the SRT is described by the free energy

$$\mathcal{F}(T,\theta) = \mathcal{F}_0(T) - \frac{1}{2}(K_a - K_c)\cos(2\theta) - \frac{1}{2}(K_4)\cos(4\theta) + \frac{\beta}{2}\left(\chi_c^2(T)F_c^2 + \chi_a^2(T)F_a^2\right) \quad (1)$$

where $\mathcal{F}_0$ is the angular independent part; θ is an angle between the uncompensated magnetization of the Fe subsystem, **F**, and the c axis; β is the constant describing the coupling between Fe and Yb moments; and $\chi \propto 1/T$ is the temperature-dependent anisotropic magnetic susceptibility tensor of the Yb moments. Due to an orthorhombic symmetry of the Fe environment, the second-order single-ion anisotropy contains two nonequivalent temperature-dependent constants K_a and K_c. The fourth-order anisotropy constant K_4 is at least an order of magnitude smaller than the second-order K_a and K_c, and plays a crucial role only in the vicinity of the SRT [29]. Assuming that the uncompensated moment of the Fe subsystem remains unchanged at the SRT, we can substitute $F_a = |F|\sin(\theta)$ and $F_c = |F|\cos(\theta)$ and rewrite Eq. (1) as

$$\mathcal{F}(T,\theta) = \mathcal{F}_0'(T) - K'(T)\cos(2\theta) - \tfrac{1}{2}(K_4)\cos(4\theta), \quad (2)$$

where the new angular independent term $\mathcal{F}_0'$ and the effective second-order anisotropy constant K' are defined as

$$\mathcal{F}_0'(T) = \mathcal{F}_0(T) + \frac{\beta|\mathbf{F}|^2}{4}\left[\chi_c^2(T) + \chi_a^2(T)\right], \quad (3)$$

$$K'(T) = \frac{1}{2}\left(K_a - K_c - \frac{\beta|\mathbf{F}|^2}{2}\left[\chi_c^2(T) - \chi_a^2(T)\right]\right). \quad (4)$$

At high temperatures the contribution of the Yb subsystem is weak and dominating K_a stabilizes the $\Gamma 4$ phase [11]. Upon cooling, the value of K' decreases because of the increase of Yb susceptibility and the SRT takes place when $K' = 0$, while the third term in Eq. (2) $\propto \cos(4\theta)$ controls the rotation of the Fe spins [11] and width of the SRT, ΔT_{SRT}. Below the SRT the $\Gamma 2$ phase is stabilized. We sketch the magnetic structures of the Fe subsystem and orientation of weak FM moment **F** with respect to crystal axes in Fig. 4(d).

By minimizing the free energy given by Eq. (2) with respect to angle θ, one can find the temperature and the width of the SRT for a given set of parameters. The minimum is achieved at $\theta = 0$ and $\pi/2$ for $\Gamma 4$ and $\Gamma 2$ phases, respectively, and gradually changes between these values within the transition region [see Fig. 4(c)]. In our paper, we use the value of the spin gap to quantify parameters of Eq. (1) and we relate the angle θ to the energy value by an empirical expression:

$$\hbar\omega(T) = \Delta_1 + \frac{2}{\pi}\Delta_2\theta(T), \quad (5)$$

where Δ_1 is the spin gap above SRT, Δ_2 is the difference between the energy gaps at $\Gamma 2$ and $\Gamma 4$ phases, and $\theta(T)$ is obtained by minimization of free energy at a given temperature.

Figure 4(a) demonstrates the temperature evolution of the energy gap of the magnon excitation close to the SRT. We fit the INS data using Eq. (5) and the results yield that the applied pressure does not affect the transition temperature

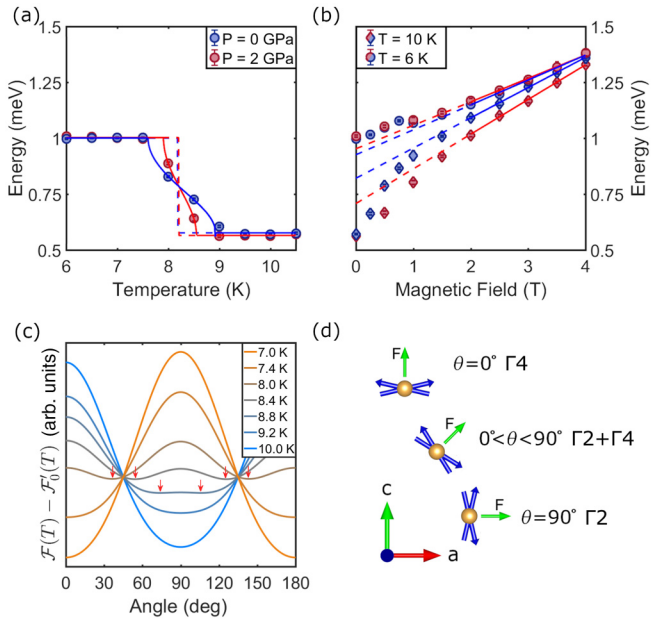

FIG. 4. (a) Energy gap at $\mathbf{Q} = (002)$ as function of temperature in the vicinity of T_{SRT}. The blue and red circles are the experimental data at ambient pressure and $p = 2$ GPa, respectively. Solid lines are the fitting results of the experimental data to the function of Eq. (5) (see text). The dashed line shows the transition in the case of $K_4 = 0$. (b) Energy gap as a function of the external magnetic field at $T = 6$ K (circles) and $T = 10$ K (squares) for the ambient pressure (blue) and $p = 2$ GPa (red), respectively. The circles and squares denote the experimental data. The lines are linear fits to the experiment for $B > 2$ T. The nonlinear behavior of the energy gap is clearly visible at low fields. (c) Angular-dependent part of free energy for different temperatures close to the SRT. Arrows indicate position of the energy minimum at intermediate temperatures. (d) Schematic representation of magnetic configuration of Fe moments and ferromagnetic moment **F** for Γ2, Γ2 + Γ4, and Γ4 phases.

$T_{\mathrm{SRT}} \approx 8.25$ K within the error bars. At the same time the transition width ΔT_{SRT} narrows under the pressure. We fitted these data using Eq. (5) and found that this effect can be directly related to the change of the K_4 parameter, which decreases by a factor of ≈ 2 at high pressure as compared to the $p = 0$ case.

In Fig. 4(b) we present the spin gap at two different temperatures above and below SRT as a function of the magnetic field. At $T = 6$ K, the curves collected at both pressures look identical within the error bars and follow a linear trend in the high-field regime, $B > 2$ T. However, interpolation of this trend towards lower fields indicates clear nonlinearity of the spin gap due to the spin-reorientation transition. At $T = 10$ K the curves collected at two pressures also follow linear dependence at high fields, $B > 2$ T, yet with a slightly different slope. However, they show a notable difference at lower fields, $B < 1.5$ T, and data collected at $p = 2$ GPa lie below the ambient pressure data. The slopes obtained from the fitting of the low-field data with a linear function are as follows.

(i) At ambient pressure, the slopes are 0.08(2) and 0.40(2) meV/T, for temperatures 6 and 10 K, respectively.

(ii) At a pressure of $p = 2$ GPa, the slopes are 0.07(1) and 0.24(1) meV/T, for temperatures 6 and 10 K, respectively.

We link this behavior to the increased width of the SRT at low pressure, enabling Fe to reorient towards the external field at a smaller external field as compared to the high-pressure case.

V. CONCLUSION

In conclusion, we successfully performed INS measurements using the combination of high pressure and magnetic field and constructed the field-temperature diagram of the spin-reorientation transition in $YbFeO_3$ at $p = 0$ and 2 GPa, based on the evolution of the energy gap of the first excitation. Our experiments have shown that when the pressure $p = 2$ GPa is applied, the transition temperature T_{SRT} remains unaffected. However, we did observe a reduction of the transition width ΔT_{SRT}. Based on the modified mean-field theory we found that this reduction can be attributed to the tuning of the fourth-order anisotropy parameter K_4 that controls the width of the transition. The K_4 decreases with pressure, which leads to the sharpness of the Γ4 → Γ2 transition. However, a whole magnetic Hamiltonian with the nontrivial microscopic interplay of the iron and rare-earth subsystems is still lacking, which calls for further studies. Overall, our paper provides important insights into the magnetic dynamics of $YbFeO_3$ and demonstrates the impact of hydrostatic pressure on the SRT.

ACKNOWLEDGMENTS

This research used resources at the Spallation Neutron Source, a U.S. Department of Energy (DOE) Office of Science User Facility operated by Oak Ridge National Laboratory. Laue x-ray diffraction measurements were conducted at the Center for Nanophase Materials Sciences (Grant No. CNMS2019-R18) at Oak Ridge National Laboratory, which is a DOE Office of Science User Facility. S.E.N. acknowledges financial support from the European Union Horizon 2020 research and innovation program under Marie Skłodowska-Curie Grant No. 884104.

[1] R. Tilley, *Perovskites: Structure-Property Relationships* (Wiley, New York, 2016).

[2] Y. Tokunaga, S. Iguchi, T. Arima, and Y. Tokura, Magnetic-Field-Induced Ferroelectric State in $DyFeO_3$, Phys. Rev. Lett. **101**, 097205 (2008).

[3] J. H. Lee, Y. K. Jeong, J. H. Park, M. A. Oak, H. M. Jang, J. Y. Son, and J. F. Scott, Spin-Canting-Induced Improper Ferroelectricity and Spontaneous Magnetization Reversal in $SmFeO_3$, Phys. Rev. Lett. **107**, 117201 (2011).

[4] Y.-J. Ke, X.-Q. Zhang, Y. Ma, and Z.-H. Cheng, Anisotropic magnetic entropy change in $RFeO_3$ single crystals (R = Tb, Tm or Y), Sci. Rep. **6**, 19775 (2016).

[5] E. Bousquet and A. Cano, Non-collinear magnetism in multiferroic perovskites, J. Phys.: Condens. Matter **28**, 123001 (2016).

[6] C. Li, S. Zheng, G. Barasa, Y. Zhao, L. Wang, C. Wang, Y. Lu, Y. Qiu, J. Cheng, and Y. Luo, A comparative study on magnetic behaviors and magnetocaloric effect in heavy rare-earth antifer-

romagnetic orthoferrites RFeO3 (R = Dy, Ho and Er), Ceram. Int. **47**, 35160 (2021).

[7] A. V. Kimel, A. Kirilyuk, P. A. Usachev, R. V. Pisarev, A. M. Balbashov, and T. Rasing, Ultrafast non-thermal control of magnetization by instantaneous photomagnetic pulses, Nature (London) **435**, 655 (2005).

[8] S. Baierl, M. Hohenleutner, T. Kampfrath, A. K. Zvezdin, A. V. Kimel, R. Huber, and R. V. Mikhaylovskiy, Nonlinear spin control by terahertz-driven anisotropy fields, Nat. Photonics **10**, 715 (2016).

[9] R. M. Bozorth, V. Kramer, and J. P. Remeika, Magnetization in Single Crystals of Some Rare-Earth Orthoferrites, Phys. Rev. Lett. **1**, 3 (1958).

[10] R. L. White, Work on the magnetic and spectroscopic properties of the rare-earth orthoferrites, J. Appl. Phys. **40**, 1061 (1969).

[11] K. P. Belov, A. K. Zvezdin, A. M. Kadomtseva, and R. Z. Levitin, Spin-reorientation transitions in rare-earth magnets, Sov. Phys. Usp. **19**, 574 (1976).

[12] F. W. Harrison, Crystal data for ytterbium orthoferrite $YbFeO_3$, Acta Cryst. **20**, 699 (1966).

[13] L. S. Wu, S. E. Nikitin, Z. Wang, W. Zhu, C. D. Batista, A. M. Tsvelik, A. M. Samarakoon, D. A. Tennant, M. Brando, L. Vasylechko, M. Frontzek, A. T. Savici, G. Sala, G. Ehlers, A. D. Christianson, M. D. Lumsden, and A. Podlesnyak, Tomonaga-Luttinger liquid behavior and spinon confinement in $YbAlO_3$, Nat. Commun. **10**, 698 (2019).

[14] S. E. Nikitin, L. S. Wu, A. S. Sefat, K. A. Shaykhutdinov, Z. Lu, S. Meng, E. V. Pomjakushina, K. Conder, G. Ehlers, M. D. Lumsden, A. I. Kolesnikov, S. Barilo, S. A. Guretskii, D. S. Inosov, and A. Podlesnyak, Decoupled spin dynamics in the rare-earth orthoferrite $YbFeO_3$: Evolution of magnetic excitations through the spin-reorientation transition, Phys. Rev. B **98**, 064424 (2018).

[15] A. Podlesnyak, S. E. Nikitin, and G. Ehlers, Low-energy spin dynamics in rare-earth perovskite oxides, J. Phys.: Condens. Matter **33**, 403001 (2021).

[16] K. P. Belov, A. K. Zvezdin, A. M. Kadomtzeva, and P. Z. Levitin, *Orientational Transitions in the Rare-Earth Magnets* (Nauka, Moscow, 1979) [in Russian].

[17] K. P. Belov, A. K. Zvezdin, A. M. Kadomtseva, and I. B. Krynetskiĭ, New orientational transitions induced in orthoferrites by an external field, Zh. Eksp. Teor. Fiz. **67**, 1974 (1974) [Sov. Phys.-JETP **40**, 980 (1975)].

[18] K. P. Belov, A. K. Zvezdin, and A. A. Mukhin, Magnetic phase transitions in terbium orthoferrite, Zh. Eksp. Teor. Fiz. **76**, 1100 (1979) [Sov. Phys. JETP **49**, 557 (1979)].

[19] Y. B. Bazaliy, L. T. Tsymbal, G. N. Kakazei, A. I. Izotov, and P. E. Wigen, Spin-reorientation in $ErFeO_3$: Zero-field transitions, three-dimensional phase diagram, and anisotropy of erbium magnetism, Phys. Rev. B **69**, 104429 (2004).

[20] Y. B. Bazaliy, L. T. Tsymbal, G. N. Kakazei, V. I. Kamenev, and P. E. Wigen, Measurements of spin reorientation in $YbFeO_3$ and comparison with modified mean-field theory, Phys. Rev. B **72**, 174403 (2005).

[21] L. T. Tsymbal, Y. B. Bazaliy, V. N. Derkachenko, V. I. Kamenev, G. N. Kakazei, F. J. Palomares, and P. E. Wigen, Magnetic and structural properties of spin-reorientation transitions in orthoferrites, J. Appl. Phys. **101**, 123919 (2007).

[22] A. Podlesnyak, M. Loguillo, G. M. Rucker, B. Haberl, R. Boehler, G. Ehlers, L. L. Daemen, D. Armitage, M. D. Frontzek, and M. Lumsden, Clamp cell with in situ pressure monitoring for low-temperature neutron scattering measurements, High Press. Res. **38**, 482 (2018).

[23] G. Ehlers, A. Podlesnyak, J. L. Niedziela, E. B. Iverson, and P. E. Sokol, The new cold neutron chopper spectrometer at the spallation neutron source: design and performance, Rev. Sci. Instrum. **82**, 085108 (2011).

[24] G. Ehlers, A. Podlesnyak, and A. I. Kolesnikov, The cold neutron chopper spectrometer at the Spallation Neutron Source: A review of the first 8 years of operation, Rev. Sci. Instrum. **87**, 093902 (2016).

[25] O. Arnold, J. C. Bilheux, J. M. Borreguero *et al.*, MANTID: Data analysis and visualization package for neutron scattering and μSR experiments, Nucl. Instrum. Methods Phys. Res., Sect. A **764**, 156 (2014).

[26] R. A. Ewings, A. Buts, M. D. Le, J. van Duijn, I. Bustinduy, and T. G. Perring, HORACE: Software for the analysis of data from single crystal spectroscopy experiments at time-of-flight neutron instruments, Nucl. Instrum. Methods Phys. Res., Sect. A **834**, 132 (2016).

[27] R. Azuah, L. Kneller, Y. Qiu, P. Tregenna-Piggott, C. Brown, J. Copley, and R. Dimeo, DAVE: A comprehensive software suite for the reduction, visualization, and analysis of low energy neutron spectroscopic data, J. Res. Natl. Inst. Stand. Technol. **114**, 341 (2009).

[28] S. E. Nikitin, S. Nishimoto, Y. Fan, J. Wu, L. S. Wu, A. S. Sukhanov, M. Brando, N. S. Pavlovskii, J. Xu, L. Vasylechko, R. Yu, and A. Podlesnyak, Multiple fermion scattering in the weakly coupled spin-chain compound $YbAlO_3$, Nat. Commun. **12**, 3599 (2021).

[29] K. Zhang, K. Xu, X. Liu, Z. Zhang, Z. Jin, X. Lin, B. Li, S. Cao, and G. Ma, Resolving the spin reorientation and crystal-field transitions in $TmFeO_3$ with terahertz transient, Sci. Rep. **6**, 1 (2016).